

Skew Incidence on Concave Wedge With Anisotropic Surface Impedance

*Original*

Skew Incidence on Concave Wedge With Anisotropic Surface Impedance / Lombardi, Guido. - In: IEEE ANTENNAS AND WIRELESS PROPAGATION LETTERS. - ISSN 1536-1225. - ELETTRONICO. - 11:(2012), pp. 1141-1145. [10.1109/LAWP.2012.2219845]

*Availability:*

This version is available at: 11583/2503796 since:

*Publisher:*

IEEE - INST ELECTRICAL ELECTRONICS ENGINEERS INC

*Published*

DOI:10.1109/LAWP.2012.2219845

*Terms of use:*

This article is made available under terms and conditions as specified in the corresponding bibliographic description in the repository

*Publisher copyright*

(Article begins on next page)

# Skew Incidence on Concave Wedge with Anisotropic Surface Impedance

Guido Lombardi, *Senior Member, IEEE*

**Abstract**—The diffraction of a plane wave at skew incidence by an arbitrary-angled concave wedge with anisotropic impedance faces is studied. Concave wedges are of interest in wireless propagation models, in particular on modeling buildings and reflectors. The solution is obtained via the generalized Wiener-Hopf technique for arbitrary impedance wedges using a numerical-analytical approach. The numerical results show the spectral properties of the fields, GTD/UTD diffraction coefficients and total fields.

**Index Terms**—Electromagnetic diffraction, electromagnetic scattering, surface impedance, wedges, uniform theory of diffraction, Wiener-Hopf method, wireless propagation.

## I. INTRODUCTION

THIS paper examines the problem of diffraction by a plane wave at skew incidence on an impenetrable concave wedge (aperture half-angle  $\Phi < \pi/2$ ) with anisotropic impedance faces immersed in an homogeneous material Fig. 1.

Scattering and diffraction by a concave wedge is of interest to the wireless community, because this geometry can model building and urban environments as well as reflectors.

We consider only time-harmonic electromagnetic fields with a time dependence specified by the factor  $e^{j\omega t}$ , which is omitted. The incident field is constituted by plane waves propagating in a medium of intrinsic impedance  $Z_o$  and having the following longitudinal components:

$$\begin{cases} E_z^i = E_o e^{j\tau_o \rho \cos(\varphi - \varphi_o)} e^{-j\alpha_o z} \\ H_z^i = H_o e^{j\tau_o \rho \cos(\varphi - \varphi_o)} e^{-j\alpha_o z} \end{cases} \quad (1)$$

where,  $\beta$  and  $\varphi_o$  are the zenithal and the azimuthal angles which define the direction of the plane wave  $\hat{k}_i$ :  $k = \omega\sqrt{\mu\epsilon}$ ,  $\alpha_o = k \cos \beta$ ,  $\tau_o = k \sin \beta$  and  $Z_o = \sqrt{\mu_o/\epsilon_o}$ .

The tensorial Leontovich boundary conditions are enforced on the two faces:

$$\begin{bmatrix} E_z(\rho, \pm\Phi) \\ E_\rho(\rho, \pm\Phi) \end{bmatrix} = \pm \mathbf{Z}_{a,b} \begin{bmatrix} H_\rho(\rho, \pm\Phi) \\ -H_z(\rho, \pm\Phi) \end{bmatrix} \quad (2)$$

The general problem of the scattering and diffraction of a plane skew electromagnetic wave by an arbitrary-angled wedge with general anisotropic impedance boundary conditions has been exhaustively dealt with the Sommerfeld-Malyuzhinets method (SM) [1]-[3] and with the Wiener-Hopf (WH) method [4]-[5] where the authors resort to approximate numerical solutions. These papers were focused on convex wedge configurations with semi-aperture angle  $\Phi \geq \pi/2$ .

G. Lombardi is with the Department of Electronics and Telecommunications, Politecnico di Torino, 10129 Torino, Italy e-mail: guido.lombardi@polito.it.

Manuscript received June 18, 2012.

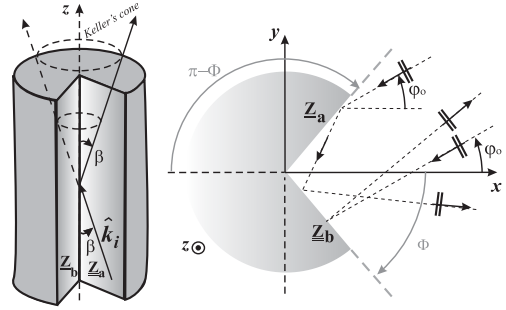


Fig. 1. The concave impenetrable wedge

Since the concave wedge presents several interesting physical aspects, in this paper we consider the most general case of concave wedge. The concave wedge problem has been only partially investigated in literature [1], [6]-[10]. In particular: [1] deals with isotropic impedance faces, [8] and [10] consider right-angled structures ( $\Phi = \pi/4$ ) with diagonal  $\mathbf{Z}_{a,b}$  matrices and, [6]-[9] investigate the *compatibility* conditions in order to avoid diffraction for  $\Phi = \pi/4$ .

This paper focuses the attention on the generation of shadow boundaries for multiple reflected components. The paper is organized as follows: Section II reviews the Wiener-Hopf formulation and its reduction to Fredholm integral equation of second kind (FIE) [4]-[5]. The same section shows the numerical solution of the FIE and also deals with the analytical continuation of the approximate representations. Section III presents the far field evaluation in term of total field by estimating: the Geometrical Optics (GO) component and the diffracted component, whereas Section IV is devoted to numerical results.

## II. FORMULATION AND SOLUTION: A REVIEW

### A. GWHE for Impenetrable Wedge Problems

Without loss of clarity we refer to the quantities reported in [4]-[5]. The generalized Wiener-Hopf equations (GWHE) for impenetrable wedge problems assumes the following form:

$$G(\eta)X_+(\eta) = X_-(m) \quad (3)$$

where  $G(\eta)$  is the matrix kernel and,  $X_+(\eta)$  and  $X_-(m)$  are the Laplace transforms of the unknown field components respectively defined for  $\varphi = 0$  in the Laplace domain  $\eta$  and for  $\varphi = \pm\Phi$  in the Laplace domain  $m$ :

$$m = -\eta \cos \Phi + \xi \sin \Phi \quad (4)$$

$$X_+(\eta) = \begin{bmatrix} V_z(\eta, 0) \\ V_\rho(\eta, 0) \\ Z_o I_z(\eta, 0) \\ Z_o I_\rho(\eta, 0) \end{bmatrix}, \quad X_-(m) = \begin{bmatrix} Z_o I_\rho(-m, \Phi) \\ -Z_o I_z(-m, \Phi) \\ -Z_o I_\rho(-m, -\Phi) \\ Z_o I_z(-m, -\Phi) \end{bmatrix} \quad (5)$$

Note that the voltages and currents are respectively Laplace transforms of the electric  $E$  and the magnetic  $H$  field components.

The reduction of GWHE to classic Wiener-Hopf equations (CWHE) is obtained via the variable transformation [4]:

$$\eta = \eta(\bar{\eta}) = -\tau_o \cos\left(\frac{\Phi}{\pi} \arccos\left(-\frac{\bar{\eta}}{\tau_o}\right)\right), \quad (6)$$

which yields

$$\bar{G}(\bar{\eta})\bar{X}_+(\bar{\eta}) = \bar{X}_-(\bar{\eta}) \quad (7)$$

in the  $\bar{\eta}$  plane.

### B. Fredholm solution of the CWHE

In this paper, instead of using the general Fredholm factorization of the WH kernel [5], we resort to the effective solution of the Fredholm integral equations in terms of the physical unknowns [12]-[11]. The integral equations are obtained by contour integration:

$$G(\bar{\eta})X_+(\bar{\eta}) + \frac{1}{2\pi j} \int_{-\infty}^{\infty} \frac{[G(u) - G(\bar{\eta})] X_+(u)}{u - \bar{\eta}} du = \bar{f}_o(\bar{\eta}) \quad (8)$$

with  $\bar{f}_o(\bar{\eta}) = \text{If}[Im[\bar{\eta}_o] < 0, \frac{R_o}{\bar{\eta} - \bar{\eta}_o}, Im[\bar{\eta}_o] > 0, \frac{G(\bar{\eta})G^{-1}(\bar{\eta}_o)F_o}{\bar{\eta} - \bar{\eta}_o}]$ .

The source coefficients  $R_o = \text{Res}\{\bar{X}_-(\bar{\eta}), \bar{\eta}_o\}$  and  $F_o = \bar{G}(\bar{\eta}_o)\text{Res}\{\bar{X}_+(\bar{\eta}), \bar{\eta}_o\}$  are obtained extracting the primary field (GO) with pole  $\bar{\eta}_o = -\tau_o \cos \frac{\Phi}{\pi} \varphi_o$  from the WH unknowns in (7). Without loss of generality we assume  $\varphi_o > 0$  and the result is that  $R_o = F_o = \{n_1, n_2, 0, 0\}/d$  where the components are reported in (9).

### C. Numerical Solution

We obtain the solution of the Fredholm equations (8) in the angular domain  $\bar{w}$  after a contour deformation [5]. We recall that  $\eta = -\tau_o \cos(w)$ ,  $\bar{\eta} = -\tau_o \cos(\bar{w})$  and  $\bar{w} = \frac{\pi}{\Phi} w$ . The contour deformation yields  $\bar{w} = -\frac{\pi}{2} + jt$ . This procedure enhances the convergence of the numerical solution obtained by simple numerical technique as uniform sampling with the interval truncation parameter  $A$  and step  $h$ . It yields:

$$H(t)Y(t) + \frac{1}{2\pi j} \int_{-\infty}^{+\infty} M(t, u)Y_i(u)du = f_o(t) \quad (10)$$

with  $H(t) = \tilde{G}(-\frac{\pi}{2} + jt) = \tilde{G}(\bar{w}) = \bar{G}(-\tau_o \cos(\bar{w}))$ ,  $Y(t) = \tilde{X}_+(-\frac{\pi}{2} + jt) = \tilde{X}_+(\bar{w}) = \bar{X}_+(-\tau_o \cos(\bar{w}))$ ,  $f_o(t) = \tilde{f}_o(-\frac{\pi}{2} + jt) = \tilde{f}_o(\bar{w}) = \bar{f}_o(-\tau_o \cos(\bar{w}))$  and

$$M(t, u) \simeq \frac{[H(u) - H(t)] \cosh u}{-\sinh u + \sinh t} \quad (11)$$

and where  $\simeq$  is an equality in the limit sense for  $u \rightarrow t$ .

In order to evaluate the far field using the Sommerfeld functions we need to estimate the unknowns in the classic  $w$  plane, therefore  $\hat{X}_+(w) = \tilde{X}_+(\frac{\pi}{\Phi} w)$ . The application of the numerical procedure yields a solution that holds for real  $w$  values only in a regularity segment  $-\Phi < w < 0$  ( $-\pi < \bar{w} < 0$ ) that belongs to the regularity strip  $P_{\bar{w}}$  defined by the image of the proper  $\bar{\eta}$  plane in the  $\bar{w}$  plane (see Figs. 13 and 14 in [5]). The regularity segment  $-\Phi < w < 0$  and regularity strip  $P_w$  for the approximate solution  $\hat{X}_{i+}^{(a)}(w)$  are then obtained using  $w = \frac{\Phi}{\pi} \bar{w}$ .

By representing the GWHE in the  $w$  plane, we perform the analytic continuation of  $\hat{X}_{i+}^{(a)}(w)$  using recursively the following expression:

$$\hat{X}_+(w) = \begin{cases} \hat{X}_+^{(a)}(w), & \text{if } w \in P_w \\ \hat{X}_+(-w), & \text{if } Re[w] > -\frac{\Phi}{2} \\ \hat{G}^{-1}(-w) \cdot \hat{G}(w - 2\Phi) \cdot \hat{X}_+(w - 2\Phi), & \text{if } Re[w] < -\frac{\Phi}{2} \end{cases} \quad (12)$$

Note that (12) returns only the first value that yields True and it is slightly different from the definition given in [5]. We have checked and reviewed this expression to extend its validity to the entire  $w$  complex plane. We note that for concave wedges ( $\Phi < \pi/2$ ) (12) must be recursively applied several times to obtain valid  $X_+(w)$  in the Sommerfeld region  $\Pi_{res}$  (the region enclosed by the SDP in  $\pm\pi$  and the Sommerfeld contour  $\gamma$ ).

### III. FAR FIELD

The longitudinal components of the fields are obtained through the Sommerfeld integral

$$\{E_z, H_z\} = \frac{1}{2\pi j} \int_{\gamma} s_{E,H}(w + \varphi) e^{+j\tau_o \cos(w)\rho} dw \quad (13)$$

where we have omitted a factor  $e^{+j\alpha_o z}$ . Eq. (13) requires the definition of the Sommerfeld functions in  $\Pi_{res}$  in terms of  $\hat{X}_+(w)$  components [13], [5]:

$$s_E(w) = \frac{j\tau_o}{2} \left[ -\sin w \hat{X}_{1+}(w) + \sin \beta \hat{X}_{4+}(w) - \cos \beta \cos w \hat{X}_{3+}(w) \right] \quad (14)$$

$$s_H(w) = \frac{j\tau_o}{2Z_o} \left[ -\sin w \hat{X}_{3+}(w) - \sin \beta \hat{X}_{2+}(w) + \cos \beta \cos w \hat{X}_{1+}(w) \right] \quad (15)$$

The total far field is then obtained as sum of GO, possible surface wave (SW) and diffracted components. The GO and the SW components derive from poles of the Sommerfeld functions evaluated at  $w + \varphi$  ( $\varphi$  is the observation angle), while the diffracted components derive from the integration of the Sommerfeld functions with argument  $w + \varphi$  along the SDP at  $\pm\pi$ . A detailed GO analysis shows that the GO poles  $w_{go}$  of  $s_{E,H}(w)$  are constituted by the incident wave pole  $w_o = -\varphi_o$  and two sets of poles related to multiple reflected waves: 1) the poles  $(-1)^n(-2n\Phi + \varphi_o)$  generated by the first reflection on face  $a$  and 2) the poles  $(-1)^n(2n\Phi + \varphi_o)$  generated by the first reflection on face  $b$ , with  $n \in \mathbb{N}_0$ . Note that each component of  $X_+(w)$  shows more poles:  $\pm 2n\Phi \pm (\mp)\varphi_o$  with  $n \in \mathbb{N}_0$ . The evaluation of GO through the residue formulas in  $w_{go} + \varphi$  avoids cumbersome expressions of the multiple reflected waves. We assert that only the last multiple two reflected waves can generate shadow boundaries (the pair with greatest  $|w_{go}|$  such that  $-\Phi < \varphi_{GO} < \Phi$  where  $\varphi_{GO} = -\text{sign}[w_{go}]\pi + w_{go}$ ). The GTD diffraction coefficients ( $D^{E,H}(\varphi, \varphi_o) = s_{E,H}(\varphi - \pi) - s_{E,H}(\varphi + \pi)$ ) show peaks only for the GO components with shadow boundaries. Only these components need uniform formulas:

$$\{E_z^d, H_z^d\} = \frac{e^{-j(\alpha_o z + \tau_o \rho + \frac{\pi}{4})}}{\sqrt{2\pi \tau_o \rho}} \cdot \left\{ D^{E,H}(\varphi, \varphi_o) + \sum_{w_{go}^{sb}} K_{w_{go}^{sb}}^{E,H} \frac{1 - F\left(2\tau_o \rho \cos^2 \frac{\varphi - w_{go}^{(sb)}}{2}\right)}{2 \cos \frac{\varphi - w_{go}^{(sb)}}{2}} \right\} \quad (16)$$

where  $w_{go}^{sb}$  are the poles of the last pair of reflected waves,  $K_{w_{go}^{sb}}^{E,H}$  are the residues of  $s_{E,H}(w)$  in  $w_{go}^{sb}$  and  $F(z)$  is the Kouyoumjian-Pathak UTD transition function [14].

$$\begin{aligned}
n_1 &= 2\pi j \sin\left(\frac{\pi\varphi_o}{\Phi}\right) \{E_o[z_{a11} \cos(\beta) \cos(\Phi - \varphi_o) - z_{a21} \sin(\beta)] - Z_o H_o[\sin(\beta) + z_{a11} \sin(\Phi - \varphi_o)]\} \\
n_2 &= 2\pi j \sin\left(\frac{\pi\varphi_o}{\Phi}\right) \{E_o[-\sin(\Phi - \varphi_o) + z_{a12} \cos(\beta) \cos(\Phi - \varphi_o) - z_{a22} \sin(\beta)] - Z_o H_o[\cos(\beta) \cos(\Phi - \varphi_o) + z_{a12} \sin(\Phi - \varphi_o)]\} \\
d &= \Phi Z_o(z_{a11} \cos^2(\beta) \cos^2(\Phi - \varphi_o) + z_{a11} \sin^2(\Phi - \varphi_o) + \sin(\beta) \sin(\Phi - \varphi_o)(z_{a11} z_{a22} - z_{a12} z_{a21} + 1) + \\
&\quad - \frac{\sin(2\beta)}{2}(z_{a12} + z_{a21}) \cos(\Phi - \varphi_o) + z_{a22} \sin^2(\beta))
\end{aligned} \tag{9}$$

#### IV. NUMERICAL RESULTS

The efficiency, the convergence and the validation of the proposed approximate solutions are illustrated through several test problems. All the test cases make reference to Fig. 1. We present several test cases making reference to what has been already published in literature. The solution has been obtained with truncation parameter  $A = 10$  and step  $h = 0.5$  [5]. In the following, all angles are in radian.

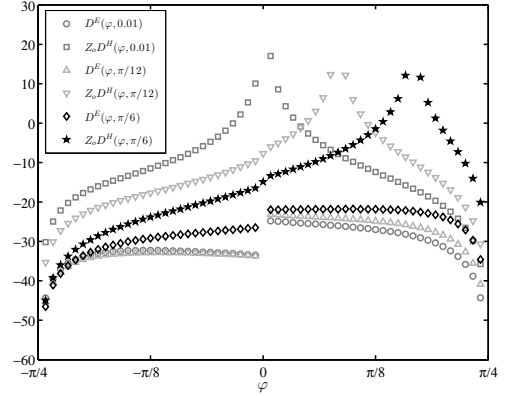
##### A. Test Case 1: Right-Angle Impedance Wedge

This test case is inspired by [10] where the GTD diffraction coefficients are shown for a right-angle impedance wedge (*i.e.*  $\Phi = \pi/4$ ) with diagonal impedance  $\mathbf{Z}_{a,b}$ . We re-propose here the test case with parameters:  $\Phi = \pi/4$ ,  $\varphi_o = \{0.01, \pi/12, \pi/6\}$ ,  $\beta = \pi/4$ ,  $z_{11}^{a,b} = 1$ ,  $z_{22}^{a,b} = 0.25$ ,  $z_{12}^{a,b} = z_{21}^{a,b} = 0$ . Fig. 2(a) shows the co-polar and cross-polar GTD diffraction coefficients in dB scale for  $E_o = 1V/m, H_o = 0A/m$ . We observe that with  $\Phi = \pi/4$  the shadow boundaries of the two double-reflected waves are coincident. In this particular test case the shadow boundary is present only in the cross-polar component, therefore Fig. 2(a) shows only one peak in  $Z_o D^H$ . The weak non singular co-polar component shows loss of convergence for  $\varphi = 0$  (due to imperfect singularity cancelation in  $X_+(w)$ ). This phenomenon does not compromise the precision of the total field as reported in Fig. 2(b). The total field is estimated with  $k\rho = 10$ ,  $k = 1 - 0.001j$ ,  $E_o = 1V/m$ ,  $H_o = 0A/m$ ,  $\varphi_o = \pi/6$ . The GO terms (reflection coefficients) are obtained via residue computation on the Sommerfeld function and are consistent with the ones obtained analytically in [10]. Similar numerical results are obtained for  $E_o = 0V/m, H_o = 1A/m$ .

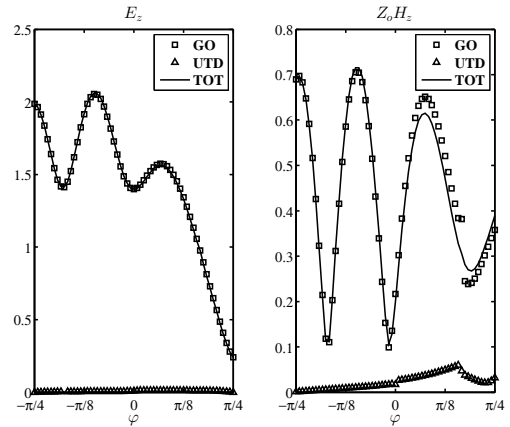
##### B. Test Case 2: Right-Angle Impedance Wedge with impedance compatibility condition

This test case is inspired by [9] where the total field is shown for a right-angle impedance wedge (*i.e.*  $\Phi = \pi/4$ ) with impedance  $\mathbf{Z}_{a,b}$  that follows the *compatibility conditions* (17) to avoid diffracted field. For the diagonal impedance case the conditions are reduced to the first constrain of (17) [6]. We propose the test case with parameters:  $\Phi = \pi/4$ ,  $\varphi_o = \pi/6$ ,  $\beta = \pi/4$ ,  $z_{11}^a = 1$ ,  $z_{22}^a = 0.2$ ,  $z_{11}^b = 1.25$ ,  $z_{22}^b = 1$ ,  $z_{12}^{a,b} = z_{21}^{a,b} = 0$ . Fig. 3 shows the co-polar and cross-polar GTD diffraction coefficients in dB scale for  $E_o = 1V/m, H_o = 0A/m$ . As expected, the GTD diffraction coefficients result in numerical noise around  $-300dB$ . We observe that no shadow boundary occurs and thus the total field is continuous.

$$\begin{aligned}
\frac{z_{22}^a}{z_{11}^a} + \frac{z_{22}^b}{z_{11}^b} &= 1; \quad z_{12}^{a,b} = -z_{21}^{a,b}; \quad z_{11}^b = \pm \sqrt{\frac{1 + \frac{z_{12}^b}{z_{11}^b} (1 - \det[\mathbf{Z}_a]) - (z_{12}^b)^2}{1 - \frac{z_{22}^a}{z_{11}^a}}} \\
\end{aligned} \tag{17}$$



(a) The co-polar  $D^E$  and cross-polar  $Z_o D^H$  GTD diffraction coefficients (dB) for  $E_o = 1V/m, H_o = 0A/m$



(b) Total fields for  $E_o = 1V/m, H_o = 0A/m$ ,  $\varphi_o = \pi/6$

Fig. 2. Test case 1.

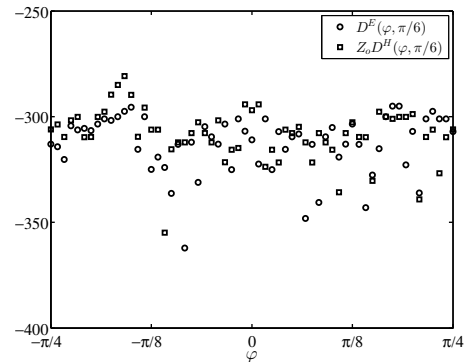


Fig. 3. Test case 2: the co-polar  $D^E$  and cross-polar  $Z_o D^H$  GTD diffraction coefficients (dB) for  $E_o = 1V/m, H_o = 0A/m$ .

##### C. Test Case 3: The Arbitrary-Angled Concave Wedge with Anisotropic Impedance Faces at Skew Incidence

This test case is the more general one. We conduct it with parameters:  $\Phi = 0.55$ ,  $\varphi_o = \pi/10$ ,  $\beta = \pi/3$ ,  $E_o = 0V/m$ ,

$Z_o H_o = 1A/m$ ,  $k = 1 - j0.001$  and

$$\mathbf{Z}_a = Z_o \begin{bmatrix} 2 & 1 + 0.5j \\ -0.5 & 10 \end{bmatrix}; \mathbf{Z}_b = Z_o \begin{bmatrix} 10 & 0 \\ 0 & 0.1 \end{bmatrix} \quad (18)$$

We note that the impedance matrices follow the constraint of passivity [15]. As shown in Fig. 4, the GO peaks in  $s_H(w)$  for  $w \in (-\pi - \Phi, \pi + \Phi)$  are seven ( $\sim \{-3.614, -1.886, -1.414, 0.314, 0.786, 2.514, 2.99\}$ ) and they are related to the incident wave and to the single, double and triple reflected waves (see Section III). The waves' coefficients are properly evaluated using the residue formula. Only the triply reflected waves generate shadow boundaries at  $\pm 6\Phi - \varphi_o \pm \pi$  as demonstrated in Fig. 5(a) where the GTD diffraction coefficient are reported. Figs. 5(b) and 5(c) show the total fields at  $k\rho = 10$ .

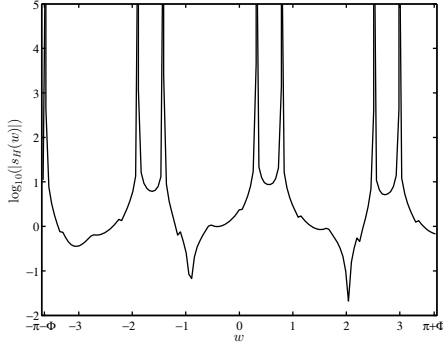


Fig. 4. Test case 3: spectral properties of  $s_H(w)$ .

## V. CONCLUSION

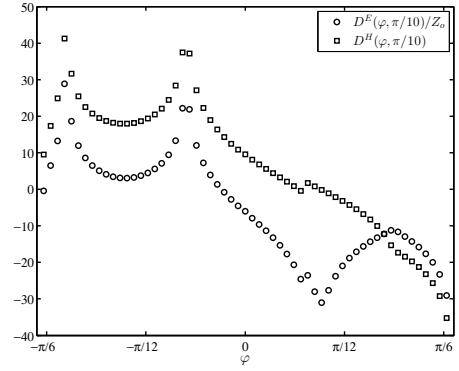
This paper presents the analysis of diffraction of a plane wave at skew incidence by an arbitrary-angle concave wedge with anisotropic impedance faces using the generalized Wiener-Hopf technique. The results show the effectiveness of the method and the field properties of the structure.

## ACKNOWLEDGMENT

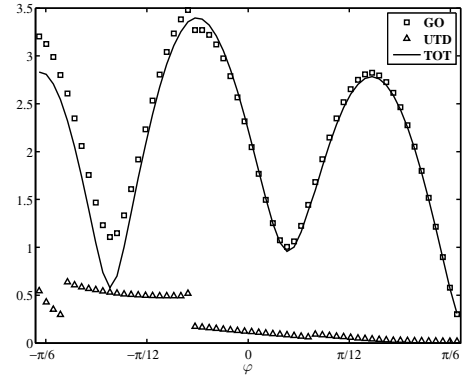
This work was supported in part by the Italian Ministry of Education, University and Research (MIUR) under PRIN Grant 20097JM7YR.

## REFERENCES

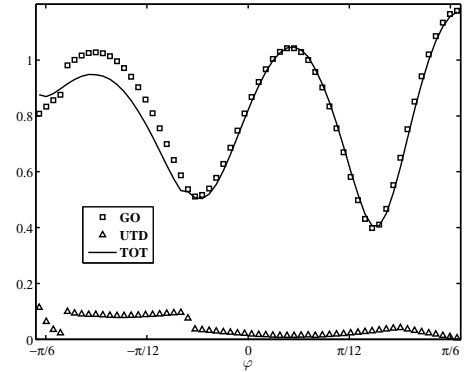
- [1] M.A. Lyalinov, N.Y. Zhu, "Diffraction of a skew incident plane electromagnetic wave by an impedance wedge," *Wave Motion*, vol. 44, pp. 21-43, 2006.
- [2] B.V. Budaev, D.B. Bogy, "Diffraction of a plane skew electromagnetic wave by a wedge with general anisotropic impedance boundary conditions," *IEEE Trans. Antennas Propag.*, vol. 54, pp. 1559-1567, May 2006.
- [3] A.V. Osipov, T.B.A. Senior, "Electromagnetic diffraction by arbitrary-angle impedance wedges," *Proc. R. Soc. A*, vol. 464, pp. 177-195, 2008.
- [4] V. Daniele, "The Wiener-Hopf technique for impenetrable wedges having arbitrary aperture angle," *SIAM J. Appl. Math.*, vol. 63, n.4, pp.1442-1460, 2003.
- [5] V. Daniele, G. Lombardi, "Wiener-Hopf Solution for Impenetrable Wedges at Skew Incidence," *IEEE Trans. Antennas Propag.*, vol. 54, n. 9, pp. 2472-2485, Sept. 2006, doi: 10.1109/TAP.2006.880723
- [6] R.B. Dybdal, L. Peters, Jr., W.H. Peake, "Rectangular waveguides with impedance walls," *IEEE Trans. Microw. Theory Tech.*, vol. 19, pp. 2-9, Jan. 1971.
- [7] T.B.A. Senior, "Skew incidence on a right-angled impedance wedge," *Radio Sci.*, vol. 13, pp. 639-647, 1978.
- [8] G. Manara, P. Nepa, G. Pelosi, A. Vallecchi, "An approximate solution for skew incidence diffraction by an interior right-angled anisotropic impedance wedge," *PIER*, Vol. 45, pp. 45-75, 2004.
- [9] T.B.A. Senior, A. V. Osipov, "Plane wave solutions for right-angled interior impedance wedges," *Radio Sci.*, vol. 42, n. RS6S04, pp. 1-8 2007.



(a) The co-polar  $D^H$  and cross-polar  $D^E/Z_o$  GTD diffraction coefficients (dB)



(b) Co-polar total field  $H_z$



(c) Cross-polar total field  $E_z/Z_o$

Fig. 5. Test case 3.

- [10] A.V. Osipov, T.B.A. Senior, "Diffraction and Reflection of a Plane Electromagnetic Wave by a Right-Angled Impedance Wedge," *IEEE Trans. Antennas Propag.*, vol.57, no.6, pp.1789-1797, June 2009
- [11] V. Daniele, *An introduction to the Wiener-Hopf Technique for the solution of electromagnetic problems*, Internal Report ELT-2004-1, Dipartimento di Elettronica, Politecnico di Torino, Sep. 2004, <http://personal.delen.polito.it/vito.daniele/>.
- [12] V. Daniele, G. Lombardi, "Fredholm factorization of Wiener-Hopf scalar and matrix kernels," *Radio Sci.*, vol. 42, no. RS6S01, pp. 1-19, 2007, doi:10.1029/2007RS003673.
- [13] V. Daniele, "Rotating Waves in the Laplace Domain for Angular Regions," *Electromagnetics*, vol. 23, n. 3, pp. 223-236, 2003.
- [14] R.G. Kouyoumjian, G. Manara, P. Nepa, B.J.E. Taute, "The diffraction of an inhomogeneous plane wave by a wedge," *Radio Sci.*, vol. 31, n. 6, pp. 1387-1397, Nov.-Dec. 1996.
- [15] N.Y. Zhu, F.M. Landstorfer, "Numerical study of diffraction and slope-diffraction at anisotropic impedance wedges by the method of parabolic equation: space waves," *IEEE Trans. Antennas Propag.*, vol. 45, n. 5, pp. 822-828, 1997.